Railway multibody simulation with the knife-edge-equivalent wheel-rail constraint equations

José L. Escalona[a,*], Javier F. Aceituno[b], Pedro Urda[a], Ole Balling[c]

[a] *Departamento de Ingeniería Mecánica y Fabricación. Universidad de Sevilla*
[b] *Departamento de Ingeniería Mecánica y Minera. Universidad de Jaén*
[c] *Department of Engineering. Aarhus University*

Abstract

This paper describes a new numerical procedure for the modelling and simulation of the wheel-rail contact in railway dynamic simulations. The method is called *knife-edge-equivalent contact constraint method* or simply *KEC-method*. Using this method, the wheel-rail contact is modelled as rigid or constraint-based using a set of kinematic constraints that eliminates one-degree of freedom of relative wheel-rail motion. The KEC-method uses a transformed but equivalent wheel profile in contact with a single-point rail. This equivalent profile has the property of producing the same wheelset-rail relative kinematics than the real wheel-rail profiles. The method can be used efficiently online while achieving better computational times than using contact lookup tables. Compared with existing constraint methods, the KEC-method has the following advantages: (1) simplification of the wheel-rail contact constraints, (2) simplified wheel-rail profiles, (3) online solution of the contact constraints, (4) reduction of the number of surface parameters and (5) increased computational efficiency. A comparative study with respect to the use of efficient contact lookup tables in the simulation of *Metro de Sevilla* (metropolitan train in the city of Sevilla) shows that this contact method is appropriate to simulate the dynamics of a railway vehicle efficiently.

*Corresponding author
Email addresses: escalona@us.es (José L. Escalona), jaceitun@ujaen.es (Javier F. Aceituno), purda@us.es (Pedro Urda), oba@eng.au.dk (Ole Balling)

Keywords: wheel-rail contact, KEC-method, simplified constraint approach, equivalent profiles, efficient multibody formulation

1. Introduction

In the dynamic simulation railway vehicles, the wheel-rail contact is the main area of investigation through the literature. It is an essential issue for analysing the dynamic behaviour of railway vehicles such as stability, curve negotiation or ride comfort [1]. The main challenge when analysing the contact between wheels and rails is the profile surfaces. The analysis results in quasi-conformal contacts leading to complex numerical evaluations of the contact point locations. The mathematical expressions of the surfaces in contact are needed for the location of the contact points and for the computation of normal and tangential contact forces. In this context, simulation tools are crucial for the design and analysis process of railway vehicle improvements. Hence, the development of efficient but accurate models that account for the wheel-rail contact solution is of great interest for railway vehicle industry developers, vehicle operators and infrastructure managers and also for researchers.

Two well-known approaches to model the wheel-rail contact can be used [2]: the constraint approach and the elastic approach. In the constraint approach, also called rigid contact, local contact deformation is neglected. The two bodies (wheel and rail) are assumed to contact in a single point without interpenetration of their volumes [3]. This kinematic condition results in non-linear algebraic equations for the contact constraints written in terms of the system coordinates and surface geometries. Normal contact forces are accounted for in the dynamic equations as the reaction associated with these constrains. In the elastic approach [4], also called penalty method, the volumes of the wheel and rail are allowed to interpenetrate. This interpenetration has to be detected through a contact search and used as an input to compute the normal contact forces. The choice of either the constraint or the elastic approach does

not affect the calculation of the tangential contact forces. Both methods have advantages and disadvantages. A good railway simulation program must implement both contact methods. Although wheel-rail contact constraints are among the most complex constrains used in the field of multibody dynamics, the constraint method is computationally more efficient than the elastic method. The main reasons are that it does not require contact search and it avoids the high-frequency oscillations associated with the very high normal stiffness of the contact surfaces applied in the elastic approach. On the other hand, wheel-rail separation (derailment scenario) and flange contact are more easily treated with the elastic method. A hybrid method that combines constraint contact in the tread and elastic contact in the flange can also be used [4],[5].

Contact geometry analysis, i.e. the determination of coinciding points or interpenetration of the surfaces, requires a high computational effort, since the mathematical descriptions of the profiles can be rather complicated and often calls for iterative solution methods. Furthermore, for some wheel/rail profile combinations sudden jump of the contact point, multiple contact points or separation of the interpenetration areas can occur, hence, it may be difficult to make sure that all solutions are found. As a consequence, vast amount of research work has been done in this field. Contact geometry analysis can be done using online or offline methods. In an online method, the contact geometry problem is solved during the numerical simulation of the entire model. Some examples can be found in [6, 7, 8, 9]. In the work of Pombo and Ambrósio [6], an elastic online contact model that allows the determination of the two-point contact scenario is presented. Malvezzi et al. [7], developed two online procedures for the detection of the contact points based on the known analytic expressions of the surfaces in contact. Also in [8], an online procedure that accounts for the track deformation in the contact point detection is proposed and in [9], a methodology that computes interpenetration areas between wheel and rail surfaces is proposed for the consideration of flexible wheel-rail contact.

In contrast, for an offline method the contact geometry is analysed in a pre-
60 processing step. The results of this analysis are the contact point location and other geometric parameters as functions of the wheelset's relative position with respect to the track. These pre-calculated results are stored in a contact lookup table; this avoids the full analysis of the contact geometry during the numerical simulation. However, its use requires simplifying assumptions associated with
65 the interpolation in the tabulated values that may decrease the accuracy of the simulation results. In the work of Escalona and Aceituno [5], a formulation to simulate the dynamics of railway vehicles using contact lookup tables that accounts for track irregularities is proposed and compared with the online solution of the contact constraints. This work shows, that dealing carefully with the
70 geometric assumptions, the use of contact lookup tables not only involves efficient simulations but also quite accurate results. Other examples of the use of contact lookup tables can be found in [10, 11]. In Sugiyama et al. [10], a hybrid offline and online approach is used for the tread and flange contact respectively and in Santamaría et al. [11], a reduced 3-DOF elastic contact lookup table is
75 presented where it is assumed that the contact point lies on radial sections at the wheel.

Another field of research in the development of efficient formulations for the multibody simulation of railway vehicles is the linearisation of the equations of motion. This is a delicate task that requires detailed understanding of the
80 vehicle motion. As an example, the equivalent conicity concept for wheel-rail contact geometry cannot be linearised for the determination of limit cycles of permanent hunting [12]. The purpose of linearisation is to considerably decrease the computational effort without compromising the accuracy of the results. As shown by Shabana et al. [13], if the small motion associated with the relative
85 motion of the bodies of the vehicle is separated from the motion associated with the vehicle forward velocity, linearisation of transformation matrices, suspension and inertia forces can be properly applied. Moreover, as there are many railway vehicle models that are developed for the analysis of either the vertical or the lateral motions (i.e. see [14, 15, 16]), the previous linearisation can be combined

with the assumption of *weakly* coupled vertical and lateral dynamics as shown by Muñoz et al. [17]. In their work the lateral and vertical dynamics are computed almost independently in a simplified railway vehicle model where the coupling between them is achieved only by the wheel-rail contact forces.

Considering the purpose of this work, special attention should be given to the work of Arnold et al. [18], Schupp et al. [19] and Netter et al. [20], where the so-called *quasi-elastic* wheel-rail contact model is proposed. In the *quasi-elastic* contact model, the elastic deformation of the contact interface is considered with the purpose of smoothing the equations of motion. The contact constraints are weighted to avoid contact point jumps. This leads to a continuous transition from tread to flange contact and to a significant reduction of the computational time. To that end, contact parameters are approximated by three-dimensional tensor product splines [18]. By smoothing the contact constraints in the case of sudden jumps of the contact points in the wheel and rail surface, the application of the method presented in this paper has similar effect in the simulations as the application of the quasi-elastic method.

With the aim of increasing the computational efficiency, this paper develops a new numerical procedure for the modelling and simulation of the wheel-rail contact named the *knife-edge equivalent contact constraint method* or simply *KEC-method* in railway dynamic simulations. The method can be used, for parameter identification [21], on-board state observation [22] or track geometry measurements [23]. The KEC-method presented here reduces the wheel-rail profiles combination to an equivalent wheel profile that contacts an ideal rail that has no lateral dimension. Hence, the equivalent wheel seems to be in contact with the edge of a knife. This method avoids the jumping of contact points (their location is given by discontinuous functions of the wheelset lateral displacement), as the *quasi-elastic* method does, but using a conceptually simpler and easily applicable method. Moreover, the KEC-method is based on a classical approach that has been used in the railway dynamics literature [24] but extended to account for the same wheelset kinematics that using real profiles. In this context, to accurately describe the dynamics of a railway vehicle, contact

forces are applied in the exact position of the real profiles because the online solution of the KEC constraints allows a direct determination of the exact position of the contact points.

The paper is organized as follows: in Section 2, railway kinematics (track and vehicle bodies) is presented and linearised to its maximum extent. Section 3 briefly details the wheel-rail profiles kinematic description. In Section 4, contact constraints are presented in its exact and approximate form together with the use of contact lookup tables. This leads to Section 5, where the knife-edge-contact constraints are derived. Its application to find the equivalent wheel profile that has the same wheelset kinematics as using the real wheel is shown in Section 6. The calculation of the wheel-rail contact forces with the KEC-method is presented in Section 7. Section 8 provides the numerical results of a railway vehicle running on a 1-km length track with irregularities to show the efficiency of the proposed method. Finally, Section 9 presents the advantages of the KEC method for the two-point contact scenario and Section 10 closes with a summary and conclusions.

2. Railway kinematics

This section describes the kinematic description of the rail geometry and the kinematic description of the bodies that move along the track (vehicle bodies). In here, rotation matrices are linearised using the small-angles assumption when this approximation is reasonable in the railway context. This approximation is not really needed for the use of the KEC-method presented in this paper. However, it results in a more efficient computational formulation with little reduction in accuracy.

2.1. Nomenclature

In this paper italic symbols represent scalar magnitudes while bold symbols represent matrices. Italic symbols with an arrow represent vector magnitudes. The use of uppercase bold symbols to represent matrix components and lower-

case to represent the components of a vector (column matrix) is not followed in this paper.

Different symbols are used to express position vectors in different frames:

- $\vec{R}$ is a position vector whose origin is attached to the global frame (GF). The GF is an inertial frame fixed in space (see Fig. 1).
- $\vec{r}$ is a position vector whose origin is attached to a track frame frame (TF), with the only exception of the irregularity vectors (see $\vec{r}^{\,lir}$ and $\vec{r}^{\,rir}$ in Figs. 2 and 3). The TF is a frame that slides along the ideal track centerline keeping the X-axis tangent to it and the Y-axis parallel to the line that connects the centre of the rail cross-sections in ideal position (see Figs. 1, 2 and 3).
- $\vec{u}$ is a position vector whose origin is attached to a body frame (BF) or rail-profile frame (RPF). The RPF is a frame located at any rail cross-section and it is used to define the rail head profile (see Fig. 3).

Vector symbols may include subscripts, representing the end-point of the position vector, and superscripts, expressing the body or frame to which they belong. In case the vector symbol does not include a subscript, it means that the end-point is the origin of the frame expressed by the superscript. Other vectors used (not position vectors) are tangent vectors to a surface, denoted by $\vec{t}$ and normal vector to a surface, denoted by $\vec{n}$.

The column matrix that contains the components of a vector in a given frame is expressed with the same symbol as the vector itself but using bold type and a different "hat" (diacritic) than an arrow. As diacritics, "bar" is used for the track frame, "arc" is used to the body frame and no diacritic is used for the global frame. As an example $\vec{R}_P^{\,i}$ is the position vector of point P that belongs to body i with respect to the global frame, $\mathbf{R}_P^i$ are the components of that vector in the GF, $\bar{\mathbf{R}}_P^i$ are the components of that vector in TF and $\hat{\mathbf{R}}_P^i$ are the

components of that vector in the BF.

Rotation matrices are expressed with symbol $\mathbf{A}$ and two superscripts separated by comma. For example, $\mathbf{A}^{t,i}$ is the transformation matrix from the BF of body i to the TF (whose symbol is t). It is easy to follow that $\bar{\mathbf{R}}_P^i = \mathbf{A}^{t,i}\hat{\mathbf{R}}_P^i$. Rotation matrices with just one superscript are rotation matrices with respect to the GF. For example $\mathbf{A}^i$ and $\mathbf{A}^t$ are the rotation matrix from the BF of body i to the GF and the rotation matrix from the TF to the GF, respectively.

2.2. Kinematics of the ideal track centreline

Track geometry is the superposition of the *ideal geometry* and the *irregularities*. The absolute position of an arbitrary point on the ideal track centreline with respect to a global frame is a function of the arc-length s, as follows:

$$\mathbf{R}^t(s) = \begin{bmatrix} R_x^t(s) \\ R_y^t(s) \\ R_z^t(s) \end{bmatrix} \tag{1}$$

where $\mathbf{R}^t$ are the components in the global frame of vector $\vec{R}^t$ shown in Fig. 1.

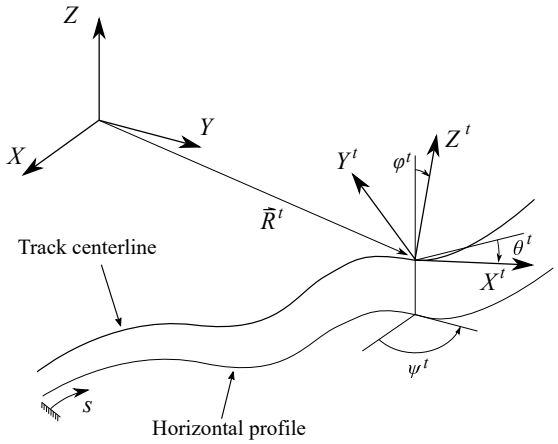

Figure 1: Track Kinematics

The track centreline geometry is characterized by the following geometric functions of the arc-length s:

- Horizontal curvature: $\rho_h(s)$
- Vertical curvature: $\rho_v(s)$
- Twist curvature: $\rho_{tw}(s)$
- Spatial-derivative of horizontal curvature: $\rho'_h(s)$
- Vertical slope: $\theta_v(s)$

The meaning of the functions is related to the fact that the geometry of the track centreline 3D-curve is defined by the *horizontal profile* and the *vertical profile* [25]. The horizontal profile is the planar curve given by the projection of the 3D-curve in the global-horizontal $X-Y$ plane (see Fig. 1). The vertical profile is the planar curve that appears when representing the height of the 3D curve with respect to the horizontal profile as a function of the arc-length s. Both profiles are defined piecewise using sections of variable length. Points between two sections are called vertices, whereby the vertices of the horizontal profile do not necessary coincide with those of the vertical profiles.

Horizontal profile sections are classified as *straight* (or *tangent*), with zero horizontal curvature, curve (circular), with constant horizontal curvature, and transitions, with variable horizontal curvature. Most common horizontal transition function is the *clothoid*, with linear space-variation of the horizontal curvature, that has been considered in this work. Each of these types of sections are described by the set of geometric parameters given in Tab. 1, where R_h is the curve radius, $f_{lin}(s)$ is a linear function of the arc-length that is zero at the straight end and one at the curved end, φ_c is the cant angle at the curved section and L_{ht} is the length of the transition.

Vertical profile sections are classified as *straight*, with zero vertical curvature, and transitions (most common vertical transition is a cubic polynomial), with non-zero horizontal curvature. Each of these types of sections are described by the set of geometric parameters given in Tab. 2, where θ_v is the vertical slope,

Straight	$\rho_h = 0$	$\rho_{tw} = 0$	$\rho'_h = 0$
Curve	$\rho_h = \frac{1}{R_h}$	$\rho_{tw} = 0$	$\rho'_h = 0$
Transition	$\rho_h = f_{lin}(s) \cdot (\frac{1}{R_h})$	$\rho_{tw} = f_{lin}(s) \cdot \varphi_c$	$\rho'_h = \frac{1}{L_{ht} \cdot R_h}$

Table 1: Section types in horizontal profile

θ_{v1} and θ_{v2} are the slopes of a straight sections before and after the transition, and L_{vt} is the length of the transition section.

Straight	$\theta_v =$ constant	$\rho_v = 0$
Transition	$\theta_v = \theta_{v1} + f_{lin}(s)(\theta_{v2} - \theta_{v1})$	$\rho_v = \frac{(\theta_{v2} - \theta_{v1})}{L_{vt}}$

Table 2: Section types in vertical profile

The list of sections of the horizontal and vertical profiles of a given track, including the value of the geometric parameters given above, allows the calculation of the function $\mathbf{R}^t(s)$ given in Eq. 1. This function uses to be implemented in a track-preprocessor that is a very important part of the railway dynamic simulation codes. The orientation of the track centreline can also be obtained as a function of s as explained next.

Figure 1 shows the frame $\langle X^t, Y^t, Z^t \rangle$ associated with the track centreline at each value of s. This frame is called here the *track frame* The orientation of the track frame with respect to a global frame can be measured with the Euler angles ψ^t (*azimuth* or *heading* angle), θ^t (vertical slope, positive when downwards in the forward direction) and φ^t (*cant* or *superelevation* angle). The azimuth ψ^t can have any arbitrary value, however, the slope θ^t and cant φ^t angles can be considered as small angles. Approximate values of the maximum slope and cant angles in railway tracks are 3.5° and 5.5°, respectively. Under these conditions, the rotation matrix from the track frame to the global frame can be approximated (linearisation of trigonometric functions of θ^t and φ^t) to:

$$\mathbf{A}^t(s) = \begin{bmatrix} \cos(\psi^t) & -\sin(\psi^t) & \theta^t\cos(\psi^t) + \varphi^t\sin(\psi^t) \\ \sin(\psi^t) & \cos(\psi^t) & \theta^t\sin(\psi^t) - \varphi^t\cos(\psi^t) \\ -\theta^t & \varphi^t & 1 \end{bmatrix} \tag{2}$$

A frame that slides along the track with a forward velocity V and a forward acceleration $\dot{V}$, while taking the same orientation as the track frame, would experience the following absolute velocity and acceleration:

$$\dot{\bar{\mathbf{R}}}^t = \begin{bmatrix} V \\ 0 \\ 0 \end{bmatrix}, \quad \ddot{\bar{\mathbf{R}}}^t = \begin{bmatrix} \dot{V} \\ \rho_h V^2 \\ -\rho_v V^2 \end{bmatrix} \tag{3}$$

where these arrays contain the first and second time-derivatives of vector $\vec{R}^t$ in the track frame. Similarly, the absolute angular velocity and the absolute angular acceleration of that body are given by:

$$\bar{\boldsymbol{\omega}}^t = \begin{bmatrix} \rho_{tw} V \\ \rho_v V \\ \rho_h V \end{bmatrix}, \quad \bar{\boldsymbol{\alpha}}^t = \begin{bmatrix} \rho_{tw}\dot{V} \\ \rho_v \dot{V} \\ \rho_h \dot{V} + \rho_h' V^2 \end{bmatrix} \tag{4}$$

where these arrays contain also the components of the angular velocity and acceleration vectors in the track frame.

2.3. Kinematics of the irregular track

Figure 2 shows the relative position of the irregular right rail centreline with respect to the track frame defined in the previous subsection. Figure 3 shows the rail heads displacement due to irregularity in a track cross-section ($Y^t - Z^t$ plane). As observed in the figure, at each railhead there is a frame defined (lrp, *left rail profile* frame, and rrp, *right rail profile* frame). The irregularity vectors $\vec{r}^{lir}$ (*lir*, *l*eft rail *ir*regularity) and $\vec{r}^{rir}$ (*rir*, *r*ight rail *ir*regularity) describe the displacement of the rail centrelines. The components of these vectors in the track frame are functions of s given by:

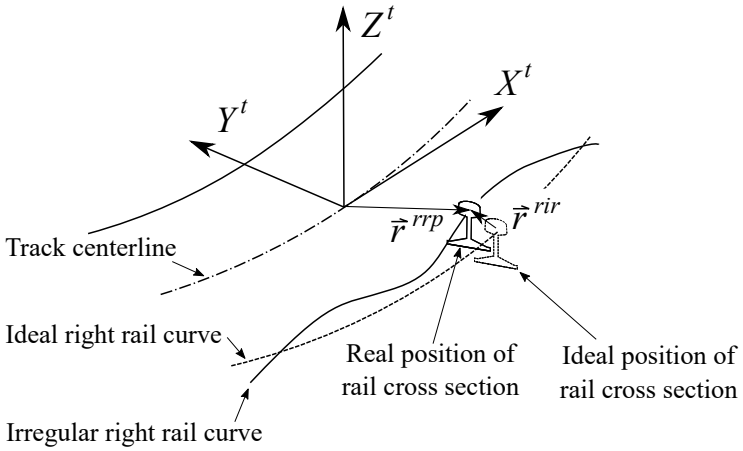

Figure 2: Rail centreline irregularity

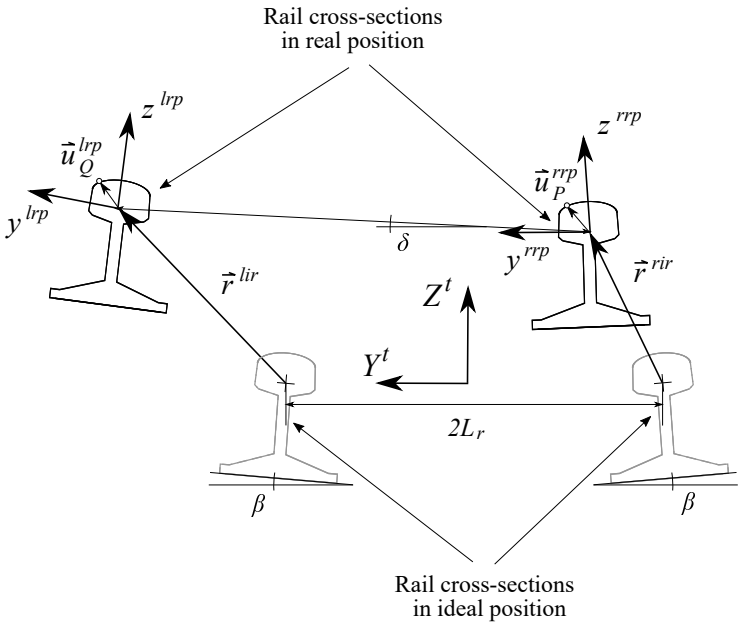

Figure 3: Kinematics of track section

$$\bar{\mathbf{r}}^{lir}(s) = \begin{bmatrix} 0 \\ y^{lir} \\ z^{lir} \end{bmatrix}, \quad \bar{\mathbf{r}}^{rir}(s) = \begin{bmatrix} 0 \\ y^{rir} \\ z^{rir} \end{bmatrix} \tag{5}$$

In the railway industry, the following four combinations of the irregularities of the rail head centrelines are measured:

- Alignment: $al = \left(y^{lir} + y^{rir}\right)/2$
- Vertical profile: $vp = \left(z^{lir} + z^{rir}\right)/2$
- Gauge variation: $gv = y^{lir} - y^{rir}$
- Cross level: $cl = z^{lir} - z^{rir}$

The orientation of the rail head frames with respect to the track frame is given by the following rotation matrices:

$$\mathbf{A}^{t,lrp}(s) = \begin{bmatrix} 1 & 0 & 0 \\ 0 & \cos(\beta+\delta) & -\sin(\beta+\delta) \\ 0 & \sin(\beta+\delta) & \cos(\beta+\delta) \end{bmatrix} \tag{6}$$

$$\mathbf{A}^{t,rrp}(s) = \begin{bmatrix} 1 & 0 & 0 \\ 0 & \cos(-\beta+\delta) & -\sin(-\beta+\delta) \\ 0 & \sin(-\beta+\delta) & \cos(-\beta+\delta) \end{bmatrix} \tag{7}$$

where β is the inclination angle of the rail profiles and $\delta = \left(z^{lir} - z^{rir}\right)/2L_r$ is the linearised rotation angle due to the irregularity. Both angles can be observed in Fig. 3.

The absolute position vectors of two points, P and Q, defined in the right and left rail heads, respectively, are given by:

$$\vec{R}_P^{rrp} = \vec{R}^t + \vec{r}^{rrp} + \vec{r}^{rir} + \vec{u}_P^{rrp} \tag{8}$$

$$\vec{R}_Q^{lrp} = \vec{R}^t + \vec{r}^{lrp} + \vec{r}^{lir} + \vec{u}_Q^{lrp} \tag{9}$$

The components of these vectors in the global frame are given by:

$$\mathbf{R}_P^{rrp} = \mathbf{R}^t + \mathbf{A}^t \left[\bar{\mathbf{r}}^{rrp} + \bar{\mathbf{r}}^{rir} + \mathbf{A}^{t,rrp} \hat{\mathbf{u}}_P^{rrp} \right] \tag{10}$$

$$\mathbf{R}_Q^{lrp} = \mathbf{R}^t + \mathbf{A}^t \left[\bar{\mathbf{r}}^{lrp} + \bar{\mathbf{r}}^{lir} + \mathbf{A}^{t,lrp} \hat{\mathbf{u}}_Q^{lrp} \right] \tag{11}$$

where $\hat{\mathbf{u}}_P^{rrp}$ and $\hat{\mathbf{u}}_Q^{lrp}$ contain the components of the position vector of points P and Q in the rail head profiles as shown in Fig. 3. These vectors are parametrized following the rail head profile geometry. Note that the uppercase symbol R in the two previous equations is used to represent the components of vectors (column matrices).

2.4. Vehicle body kinematics

A "vehicle body" means here any body belonging to the vehicle, not necessary the car body. The generalized coordinates used to describe the position and orientation of body i that moves along the track are:

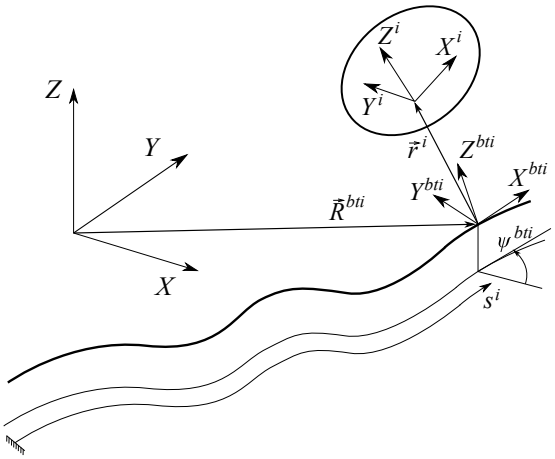

Figure 4: Kinematics of a vehicle body along the track

$$\mathbf{q}^i = \begin{bmatrix} s^i \\ y^i \\ z^i \\ \varphi^i \\ \theta^i \\ \psi^i \end{bmatrix} \tag{12}$$

where s^i defines the position along the track of the body, y^i and z^i define the position of the body with respect to the track centreline, see Fig. 4, and φ^i, θ^i and ψ^i define the orientation of the body frame with respect to the track frame in a $X-Y-Z$ sequence, respectively. Once the arc-length s^i is given, one can compute the position and orientation of the *body-track frame* i as follows:

$$\mathbf{R}^{bti} = \mathbf{R}^t\left(s = s^i\right), \quad \mathbf{A}^{bti} = \mathbf{A}^t\left(s = s^i\right) \tag{13}$$

The components of the position vector of the body frame with respect to the body track frame are:

$$\bar{\mathbf{r}}^i = \begin{bmatrix} 0 \\ y^i \\ z^i \end{bmatrix} \tag{14}$$

And the orientation matrix of the body frame with respect to the body-track frame, that has been linearised using the small-angles assumption, is given by:

$$\mathbf{A}^{bti,i} = \begin{bmatrix} 1 & -\psi^i & \theta^i \\ \psi^i & 1 & -\varphi^i \\ -\theta^i & \varphi^i & 1 \end{bmatrix} \tag{15}$$

The absolute position vector of an arbitrary point P of body i is given by:

$$\vec{R}_P^i = \vec{R}^{bti} + \vec{r}^i + \vec{u}_P^i \tag{16}$$

The components of this vector in the global frame are given by:

$$\mathbf{R}_P^i = \mathbf{R}^{bti} + \mathbf{A}^{bti}\left[\bar{\mathbf{r}}^i + \mathbf{A}^{bti,i}\hat{\mathbf{u}}_P^i\right] \tag{17}$$

These components are determined by the value of the coordinates $\mathbf{q}^i$ and the local position vector $\hat{\mathbf{u}}_P^i$ that define the position of P within the body.

2.5. Wheelset kinematics

The wheelset treated in this subsection is the conventional railway component that includes two profiled wheels rigidly connected by an axle. The kinematic description of the equivalent component with independently rotating wheels (IRW), called here *IRW-wheelset*, that is also modelled and simulated in Section 8 of this paper, does not follow the method presented in this subsection. Wheelsets are considered as solids of revolution, such that, rotation about their axis of symmetry does not change their contour. As any other body in the railway vehicle, the position and orientation of wheelset i are given by the following set of generalized coordinates:

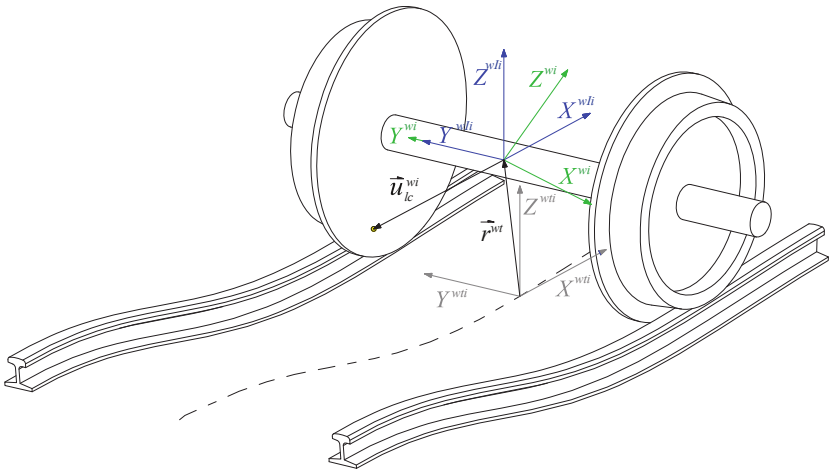

Figure 5: Kinematics of a wheelset

$$\mathbf{q}^{wi} = \begin{bmatrix} s^{wi} \\ y^{wi} \\ z^{wi} \\ \varphi^{wi} \\ \theta^{wi} \\ \psi^{wi} \end{bmatrix} \tag{18}$$

However, in contrast to the pitch angle θ^i of the other bodies, which describes small oscillations around zero, the rolling angle θ^{wi} of the wheelset increases due to the overturning, while the wheelset is travelling along the track. Therefore, the rolling angle θ^{wi} of the wheelset cannot be considered as a small angle and kinematic linearisation of this rotation is not admissible. Due to this fact, and in order to take advantage of the axisymmetric shape of the wheels, it is convenient to define an additional frame for each wheelset, called the *wheelset intermediate frame*, wIi, that performs all rotations of the wheelset except the rolling motion with the angle θ^{wi}. Figure 5 shows the wheelset i body frame wi and the intermediate one wIi. The wheelset intermediate frame wIi is defined using a sequence of rotations X-Z with respect to the wheelset-track frame wti, such that the corresponding angles φ^{wi} and ψ^{wi} can be assumed to be small and kinematic linearisation is valid. Under these conditions, the orientation of the wheelset body frame wi with respect to the wheelset track frame wti is given by the following matrix:

$$\mathbf{A}^{wti,wi} = \mathbf{A}^{wti,wIi}\mathbf{A}^{wIi,wi} = \begin{bmatrix} 1 & -\psi^{wi} & 0 \\ \psi^{wi} & 1 & -\varphi^{wi} \\ 0 & \varphi^{wi} & 1 \end{bmatrix} \begin{bmatrix} \cos\left(\theta^{wi}\right) & 0 & \sin\left(\theta^{wi}\right) \\ 0 & 1 & 0 \\ -\sin\left(\theta^{wi}\right) & 0 & \cos\left(\theta^{wi}\right) \end{bmatrix} \tag{19}$$

This way, the large angle θ^{wi}, that is left as the last one in the sequence that describes the rotation of the wheelset with respect to the wheelset-track frame, is defined with respect to an axis that coincides with the axis of symmetry of the geometry of the wheels. Due to these reasons, the wheel profile geometry can

be defined in the wheelset intermediate frame as simply as it is defined in the wheelset body frame. These properties of the wheelset intermediate frame will be exploited in next section where the wheel-rail contact constraint equations are described.

3. Contact geometry

This section describes the kinematic description of the wheel and rail head profiles. Figure 6 shows the surface parameters and profile functions that are used to locate points in the surface of the wheels or rail heads.

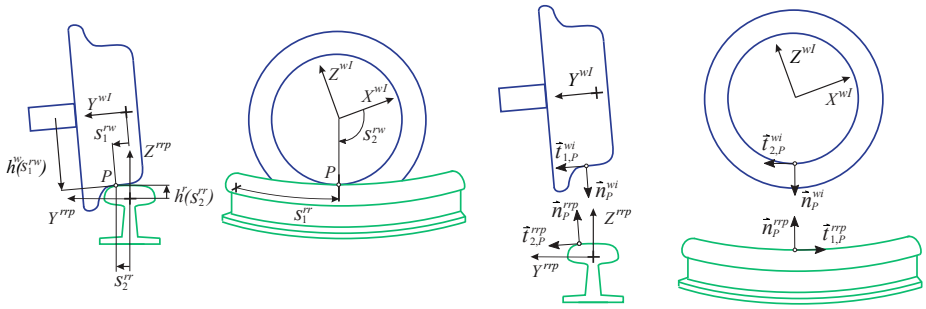

Figure 6: Wheel-rail contact geometry

Vectors $\vec{u}_P^{\,rrp}$ or $\vec{u}_Q^{\,lrp}$ are given in the rail profile frame by the following functions:

$$\hat{\mathbf{u}}_P^{rrp} = \begin{bmatrix} 0 \\ s_2^{rr} \\ h^r\left(s_2^{rr}\right) \end{bmatrix}, \quad \hat{\mathbf{u}}_Q^{lrp} = \begin{bmatrix} 0 \\ s_2^{lr} \\ h^r\left(s_2^{lr}\right) \end{bmatrix} \tag{20}$$

where lr and rr stand for 'left rail' and 'right rail', and h^r is the function that defines the rail head profile. Surface parameters s_2^{lr} and s_2^{rr} (see Fig. 6) are the left and right transverse rail surface parameters, respectively.

The position of an arbitrary point in the surface of the left or right wheel is given in the wheelset intermediate frame by:

$$\hat{\mathbf{u}}_P^{wi} = \begin{bmatrix} h^{rw}\left(s_1^{rw}\right)\cos\left(s_2^{rw}\right) \\ -L_w + s_1^{rw} \\ -h^{rw}\left(s_1^{rw}\right)\sin\left(s_2^{rw}\right) \end{bmatrix}, \quad \hat{\mathbf{u}}_Q^{wi} = \begin{bmatrix} h^{lw}\left(s_1^{lw}\right)\cos\left(s_2^{lw}\right) \\ L_w + s_1^{lw} \\ -h^{lw}\left(s_1^{lw}\right)\sin\left(s_2^{lw}\right) \end{bmatrix} \tag{21}$$

where lw and rw stand for 'left wheel' and 'right wheel', h^{rw} and h^{lw} are the functions that define the right and left wheel profiles and L_w is the distance from the wheelset axle centre to the centre of the wheels where the origin of the wheel profiles is defined. Surface parameters s_1^{lw} and s_1^{rw} (see Fig. 6) are the left and right transverse wheel surface parameters, respectively, and s_2^{lw} and s_2^{rw} (see Fig. 6) are the left and right angular wheel surface parameters, respectively. Note that the angular parameters are defined with respect to the wheelset intermediate frame. Also note that, in the description of the wheel profile and rail head geometry, symbol s is used for all parameters regardless of being a translational magnitude or an angular one.

The functions provided in Eqs. 20 and 21 can be used to obtain two tangents and the normal vector to the surfaces of the wheel and the rail, as follows:

$$\hat{\mathbf{t}}_{1,P}^{rrp} = \begin{bmatrix} 1 \\ 0 \\ 0 \end{bmatrix}, \quad \hat{\mathbf{t}}_{2,P}^{rrp} = \begin{bmatrix} 0 \\ 1 \\ h'^{r}\left(s_2^{rr}\right) \end{bmatrix}, \quad \hat{\mathbf{n}}_P^{rrp} = \hat{\mathbf{t}}_{1,P}^{rrp} \times \hat{\mathbf{t}}_{2,P}^{rrp} \tag{22}$$

$$\hat{\mathbf{t}}_{1,Q}^{lrp} = \begin{bmatrix} 1 \\ 0 \\ 0 \end{bmatrix}, \quad \hat{\mathbf{t}}_{2,Q}^{lrp} = \begin{bmatrix} 0 \\ 1 \\ h'^{r}\left(s_2^{rr}\right) \end{bmatrix}, \quad \hat{\mathbf{n}}_Q^{lrp} = \hat{\mathbf{t}}_{1,Q}^{lrp} \times \hat{\mathbf{t}}_{2,Q}^{lrp} \tag{23}$$

$$\hat{\mathbf{t}}_{1,P}^{wi} = \begin{bmatrix} h'^{rw}\left(s_1^{rw}\right)\cos\left(s_2^{rw}\right) \\ 1 \\ -h'^{rw}\left(s_1^{rw}\right)\sin\left(s_2^{rw}\right) \end{bmatrix}, \quad \hat{\mathbf{t}}_{2,P}^{wi} = \begin{bmatrix} -h^{rw}\left(s_1^{rw}\right)\sin\left(s_2^{rw}\right) \\ 0 \\ -h^{rw}\left(s_1^{rw}\right)\cos\left(s_2^{rw}\right) \end{bmatrix} \tag{24}$$

$$\hat{\mathbf{t}}_{1,Q}^{wi} = \begin{bmatrix} h'^{lw}\left(s_1^{lw}\right)\cos\left(s_2^{lw}\right) \\ 1 \\ -h'^{lw}\left(s_1^{lw}\right)\sin\left(s_2^{lw}\right) \end{bmatrix}, \quad \hat{\mathbf{t}}_{2,Q}^{wi} = \begin{bmatrix} -h^{lw}\left(s_1^{lw}\right)\sin\left(s_2^{lw}\right) \\ 0 \\ -h^{lw}\left(s_1^{lw}\right)\cos\left(s_2^{lw}\right) \end{bmatrix} \tag{25}$$

$$\hat{\mathbf{n}}_P^{wi} = \hat{\mathbf{t}}_{1,P}^{wi} \times \hat{\mathbf{t}}_{2,P}^{wi}, \quad \hat{\mathbf{n}}_Q^{wi} = \hat{\mathbf{t}}_{1,Q}^{wi} \times \hat{\mathbf{t}}_{2,Q}^{wi} \tag{26}$$

where all tangent vectors $\hat{\mathbf{t}}$ are obtained as partial derivatives of local position vectors with respect to the surface parameters as follows: $\hat{\mathbf{t}}_{i,R}^{j} = \partial \hat{\mathbf{u}}_R^j \big/ \partial s_i^j$, being $j = wi$, lrp or rrp, $i = 1$ or 2 and $R = P$ or Q.

4. Contact constraints

The wheel-rail contact can be modelled using contact constraints. These constraints are geometric conditions that the two bodies in contact have to fulfil under the assumptions of non-conformal contact. Non-conformal contact, as it is assumed in the classical Hertz contact theory, applies if the geometry of the bodies in contact is smooth and the local curvatures about the contact points of the two surfaces are different. Under these conditions, contact between the two bodies appears in a single point (no contact patch) in the absence of deformation. Contact constraints are not related to the relative velocity of the contact points. This is, two bodies that fulfil the contact constraints can roll-without-slip (pure rolling) or they can roll and slip and spin also. The forces associated with the relative velocity of the contact points (tangential contact forces or *creep forces* as they use to be called in railway applications) are treated in the equations of motion as applied forces, as explained at the end of Section 7 of this paper. However, normal contact forces are accounted for as reaction forces associated with the contact constraints.

4.1. Exact contact constraints

In the most general form, for each wheel-rail contact, 5 non-linear algebraic equations, called contact constraints, can be defined. These equations are written in terms of the 6 wheelset coordinates $\mathbf{q}^{wi}$ and the wheel and rail surface parameters that define the local position the contact point in the wheel and the rail (4 additional *non-generalized coordinates*). Therefore, each wheel-rail contact eliminates one degree of freedom to the motion of the wheelset, because

it adds 4 variables (surface parameters) but also 5 nonlinear algebraic equations that have to be fulfilled. A wheelset with two wheels in contact with the rails has 4 degree of freedom: 6 generalized coordinates in $\mathbf{q}^{wi}$, plus 8 surface parameters for the location of the left and right wheel-rail contacts, that has to fulfil 10 nonlinear algebraic equations ($6 + 8 - 10 = 4$).

The constraint equations are the 3 *contact-point position constraints* and the 2 *tangent-plane orientation constraints*. Contact-point position constraints establish that the absolute position of the contact point in the rail is the same than the absolute position of the contact point in the wheel. Tangent-plane orientation constraints establish that the tangent plane to the rail at the contact point is parallel to the tangent plane to the wheel at the contact point. These last constraints are defined by making the dot product of two tangent vectors to the surface of the wheel by the normal vector to the surface of the rail to be zero. Figure 7 shows a 2D view of the surfaces of the wheel and rail in contact at point C. The contact constraint equations yield:

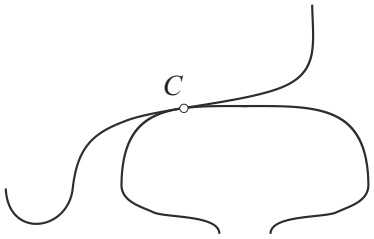

Figure 7: Wheel and rail in contact

$$\mathbf{R}_c^{wi}\left(\mathbf{q}^{wi}, \mathbf{s}^{w}\right) - \mathbf{R}_c^{rp}\left(\mathbf{s}^{r}\right) = \mathbf{0} \tag{27}$$

$$\left[\mathbf{t}_{1,c}^{wi}\left(\mathbf{q}^{wi}, \mathbf{s}^{w}\right)\right]^T \mathbf{n}_c^{rp}\left(\mathbf{s}^{r}\right) = 0 \tag{28}$$

$$\left[\mathbf{t}_{2,c}^{wi}\left(\mathbf{q}^{wi}, \mathbf{s}^{w}\right)\right]^T \mathbf{n}_c^{rp}\left(\mathbf{s}^{r}\right) = 0 \tag{29}$$

where c can be lc (left contact) or rc (right contact), w can be lw (left wheel) or rw (right wheel), rp can be lrp (left rail profile) or rrp (right rail profile), and

$\mathbf{s}^w = [s_1^w \quad s_2^{lw}]^T$ and $\mathbf{s}^r = [s_1^r \quad s_2^r]^T$ contain the surface parameters associated with the contact point in the wheel and the rail, respectively. In these equations, the absolute components of the position, tangent and normal vectors, using the kinematic description derived in the previous sections, are given by:

$$\mathbf{R}_c^{wi} = \mathbf{R}^{wti}\left(s^{wi}\right) + \mathbf{A}^{wti}\left(s^{wi}\right)\left[\bar{\mathbf{r}}^{wi}\left(\mathbf{q}^{wi}\right) + \mathbf{A}^{wti,wIi}\left(\mathbf{q}^{wi}\right)\hat{\mathbf{u}}_c^{wi}\left(\mathbf{s}^w\right)\right] \tag{30}$$

$$\mathbf{R}_c^{rp} = \mathbf{R}^{t}\left(s_1^r\right) + \mathbf{A}^{t}\left(s_1^r\right)\left[\bar{\mathbf{r}}^{lrp} + \bar{\mathbf{r}}^{irr}\left(s_1^r\right) + \mathbf{A}^{t,rp}\left(s_1^r\right)\hat{\mathbf{u}}_c^{rp}\left(s_2^r\right)\right] \tag{31}$$

$$\mathbf{t}_{1,c}^{wi} = \mathbf{A}^{wti}\left(s^{wi}\right)\mathbf{A}^{wti,wIi}\left(\mathbf{q}^{wi}\right)\hat{\mathbf{t}}_{1,c}^{wi}\left(\mathbf{s}^w\right) \tag{32}$$

$$\mathbf{t}_{2,c}^{wi} = \mathbf{A}^{wti}\left(s^{wi}\right)\mathbf{A}^{wti,wIi}\left(\mathbf{q}^{wi}\right)\hat{\mathbf{t}}_{2,c}^{wi}\left(\mathbf{s}^w\right) \tag{33}$$

$$\mathbf{n}_c^{rp} = \mathbf{A}^{t}\left(s_1^r\right)\mathbf{A}^{t,rp}\left(s_1^r\right)\hat{\mathbf{n}}_c^{rp}\left(s_2^r\right) \tag{34}$$

where the functional dependency is written in brackets. Note that the rolling angle of the wheelset θ^{wi} (the one that cannot be linearised) does not appear into these equations because the wheel geometry has been described in the wheelset intermediate frame.

4.2. Approximate contact constraints

The contact constraints given in Eqs. 27-29 are simplified using the following geometric assumptions:

1. The track cross-section that contains the centre of the wheelset also contains the left and right rail contact points, this is: $s^{wi} = s_1^{rr} = s_1^{lr}$.
2. The contact points on the left and right rail wheel profiles are contained in the $Y^{wIi} - Z^{wIi}$ plane, this is, $s_2^{lw} = s_2^{rw} = \pi/2$ rad.

The above assumptions are equivalent to neglect the influence of the wheelset yaw angle ψ^{wi} on the location of the contact points. As demonstrated in [5], these assumptions are accurate enough even in the case of tracks with narrow curves ($R = 165$ m), in which wheelsets show relatively high yaw angles up to 16 mrad. In practical terms, the above assumptions reduces the general 3D contact problem that involves surfaces contact to an equivalent 2D contact problem that involves curves contact. In other words, the location of the contact point that requires $2+2=4$ surface parameters in the general case only requires $1+1=2$ surface parameters when using the above assumptions. These are the transverse contact parameters on the rail s_2^r and the wheel s_1^w that will be simply called s^r and the wheel s^w from now on, where $r = lr$ or rr and $w = lw$ or rw.

The simplifying assumptions have more consequences related to the contact constraints. Since the number of coordinates is reduced by 2 (two surface parameters are fixed in each of the contacts) the number of constraints has to be reduced by 2 also to keep the same number of degrees of freedom of the wheelset. In addition, fixing the track cross-section where the contacts occur allows to write the contact constraints in the wheelset-track frame, as follows:

$$\bar{\mathbf{r}}_c^{wi}\left(\mathbf{q}^{wi}, s^w\right) - \bar{\mathbf{r}}_c^{rp}\left(s^r\right) = \mathbf{0} \tag{35}$$

$$\left[\bar{\mathbf{t}}_c^{wi}\left(\mathbf{q}^{wi}, s^w\right)\right]^T \bar{\mathbf{n}}_c^{rp}\left(s^r\right) = 0 \tag{36}$$

where Eq. 35 just contain the Y and Z components of the vectors (two equations) and the tangent used in Eq. 36 is the one in the transverse direction $\bar{\mathbf{t}}_c^{wi} = \bar{\mathbf{t}}_{1,c}^{wi}$. In these equations, the components of the position, tangent and normal vectors in the wheelset-track frame are given by:

$$\bar{\mathbf{r}}_c^{wi} = \bar{\mathbf{r}}^{wi}\left(\mathbf{q}^{wi}\right) + \mathbf{A}^{wti,wIi}\left(\mathbf{q}^{wi}\right)\hat{\mathbf{u}}_c^{wi}\left(s^w\right) \tag{37}$$

$$\bar{\mathbf{r}}_c^{rp} = \bar{\mathbf{r}}^{lrp} + \bar{\mathbf{r}}^{irr}\left(s^{wi}\right) + \mathbf{A}^{t,rp}\left(s^{wi}\right)\hat{\mathbf{u}}_c^{rp}\left(s^r\right) \tag{38}$$

$$\bar{\mathbf{t}}_c^{wi} = \mathbf{A}^{wti,wIi}\left(\mathbf{q}^{wi}\right)\hat{\mathbf{t}}_c^{wi}\left(s^w\right) \tag{39}$$

$$\bar{\mathbf{n}}_c^{rp} = \mathbf{A}^{t,rp}\left(s^{wi}\right)\hat{\mathbf{n}}_c^{rp}\left(s^r\right) \tag{40}$$

It can be observed that the level of simplification that can be achieved with the geometric assumptions is very high: not only the number of constrains and coordinates are reduced by 2 but the computation of the terms involved in these equations, as given in Eqs. 37-40, is greatly simplified too.

In the case of a wheelset that requires two sets of wheel-rail contact constraints, Table 3 summarizes the simplification achieved with the approximate contact constraints (third row) with respect to the exact ones (second row). In this table, the second column gives the frame where the vectors involved in the equations are resolved, the third column shows the number of scalar constraint equations that has to be defined and the fourth columns shows the number of geometric parameters involved in the constraint equations.

Table 3: Simplification of contact constraints

Form	**Frame**	**Number of C**	**Number of s**
Exact	Global	10	8
Approximate	Track	6	4
KEC	Track	4	2

4.3. Contact lookup tables

The simplified constraint equations of Eqs. 35-36 can be solved with the help of contact lookup tables in a very computationally-efficient manner [5]. Because these equations are written in the wheelset-track frame, the influence of the wheelset arc-length s^{wi} is just due to the existence of rail irregularities whose values depend on the arc-length along the track. The arc-length s^{wi}

is needed to compute the value of the components of $\mathbf{r}^{ir}$ and $\mathbf{A}^{t,rp}$. In an irregularity-free track, Eqs. 35-36 do not depend on s^{wi}.

As it is now demonstrated, the wheelset yaw angle ψ^{wi} does not have any influence in the simplified constraint equations of Eqs. 35-36 either. Even though the yaw angle ψ^{wi} is used to calculate the rotation matrix $\mathbf{A}^{wti,wIi}$, as shown in Eq. 19, substituting the assumption $s_2^{lw} = s_2^{rw} = \pi/2$ in Eqs. 21, 24-25 yields:

$$\mathbf{A}^{wti,wIi}\hat{\mathbf{u}}_c^{wi} = \begin{bmatrix} 1 & -\psi^{wi} & 0 \\ \psi^{wi} & 1 & -\varphi^{wi} \\ 0 & \varphi^{wi} & 1 \end{bmatrix} \begin{bmatrix} 0 \\ \pm L_w + s^w \\ -h^w\left(s^w\right) \end{bmatrix} = \begin{bmatrix} -\psi^{wi}\left[\pm L_w + s^w\right] \\ \pm L_w + s^w + \varphi^{wi} h^w\left(s^w\right) \\ \varphi^{wi}\left[\pm L_w + s^w\right] - h^w\left(s^w\right) \end{bmatrix} \tag{41}$$

$$\mathbf{A}^{wti,wIi}\hat{\mathbf{t}}_c^{wi} = \begin{bmatrix} 1 & -\psi^{wi} & 0 \\ \psi^{wi} & 1 & -\varphi^{wi} \\ 0 & \varphi^{wi} & 1 \end{bmatrix} \begin{bmatrix} 0 \\ 1 \\ -h'^w\left(s^w\right) \end{bmatrix} = \begin{bmatrix} -\psi^{wi} \\ 1 + \varphi^{wi} h'^w\left(s^w\right) \\ \varphi^{wi} - h^w\left(s^w\right) \end{bmatrix} \tag{42}$$

The Y and Z components of these two arrays, which are the ones used in the simplified contact constraints, do not depend on ψ^{wi}.

Finally, because the contact geometry on the wheel is axisymmetric and it is resolved in the wheelset intermediate frame, the constraint equations do not depend on the rolling angle θ^{wi} either. This property it not the result of a simplification and it can be exploited in any form of the constraint equations. It can be concluded that in an irregularity-free track, the simplified constrain equations Eqs. 35-36 depend on 3 $(y^{wi}, z^{wi}, \varphi^{wi})$ out of the 6 generalized coordinates of the wheelset given in Eq. 18.

To create a contact lookup table, a set of discrete numerical values is assigned to the lateral displacement of the wheelset y^{wi} in a range of reasonable limits. The range starts in a position with flange climb in the right wheel and ends in a position with flange climb the left wheel passing through the centred position $(y^{wi} = 0)$. For each of these positions 6 simplified contact constraints (3 for left

contact and 3 for right contact) are solved to find the values of 6 coordinates: the wheelset position and orientation coordinates z^{wi} and φ^{wi} and the surface parameters s^{lw}, s^{rw}, s^{lr} and s^{rr} needed to locate the contact points on the left and right wheel and rail surfaces. The contact lookup table can be interpreted as a set of tabulated functions of the form:

$$z^{wi} = z^{clu}\left(y^{wi}\right), \quad \varphi^{wi} = \varphi^{clu}\left(y^{wi}\right) \tag{43}$$

$$s^{lw} = s^{clu}\left(y^{wi}\right), \quad s^{rw} = s^{clu}\left(y^{wi}\right), \quad s^{lr} = s^{clu}\left(y^{wi}\right), \quad s^{rr} = s^{clu}\left(y^{wi}\right) \tag{44}$$

where the superscript clu stands for '*c*ontact *l*ook*u*p table'. The contact lookup table can be used in dynamic simulations to find the values of these six coordinates from the value of the lateral displacement. Practical use of the contact lookup tables is explained in [5].

In order to deal with a track with irregularities, the contact lookup table has to be extended from 1 entry to 2 entries. The process of creation of the contact lookup table has to be repeated for a set of values of the gauge variation (gv) within a reasonable range. This is, the contact lookup table is recalculated a number of times after approaching and separating the rails from the nominal distance $2L_r$ shown in Fig. 3. That way, the functions given above become functions of two variables, as follows:

$$\bar{z}^{wi} = z^{clu}\left(\bar{y}^{wi}, gv\right), \quad \bar{\varphi}^{wi} = \varphi^{clu}\left(\bar{y}^{wi}, gv\right) \tag{45}$$

$$s^{lw} = s^{clu}\left(\bar{y}^{wi}, gv\right), \quad s^{rw} = s^{clu}\left(\bar{y}^{wi}, gv\right), \quad s^{lr} = s^{clu}\left(\bar{y}^{wi}, gv\right), \quad s^{rr} = s^{clu}\left(\bar{y}^{wi}, gv\right) \tag{46}$$

The use of the lookup tables with irregular track is slightly different. In a dynamic simulation, given the longitudinal position of the wheelset s^{wi}, the values of the irregularities al, vp, gv and cl can be obtained. The lateral displacement that has to be used to enter the lookup table is not y^{wi}, that gives the lateral displacement with respect to the ideal track centreline, but $\bar{y}^{wi} = y^{wi} - al$, that gives the lateral displacement with respect to the irregular track centreline. In

turn, the outputs of the lookup table ($\bar{z}^{wi}$ and $\bar{\varphi}^{wi}$) have to be interpreted differently, being $z^{wi} = \bar{z}^{wi} + vp$ and $\varphi^{wi} = \bar{\varphi}^{wi} + cl/2L_r$. More details about the use of the contact lookup tables with irregularities can be found in [5].

5. Knife-edge contact constraints

Figure 8 shows a wheelset in contact with a track whose rail heads are assumed as single points, with zero width. This is what it is called here a knife-edge contact, because the rail heads are assumed as the edge of a knife. Because of this property, the location of the contact point on the knife-edge rail head is known. For the knife-edge contact constraints (*KEC constraints*) only the condition of the coincidence of two points belonging to the two surfaces, as expressed in Eq. 27, has to be fulfilled. The orthogonality condition for the normal vector of one surface and the tangential vectors of the other one, as formulated in Eqs. 28-29, cannot be applied here, since for the cross section of the knife edge no tangential vectors and therefore no normal vectors are defined. It is evident that this leads to a simpler formulation of the contact constraints and thereby to a reduced computational effort.

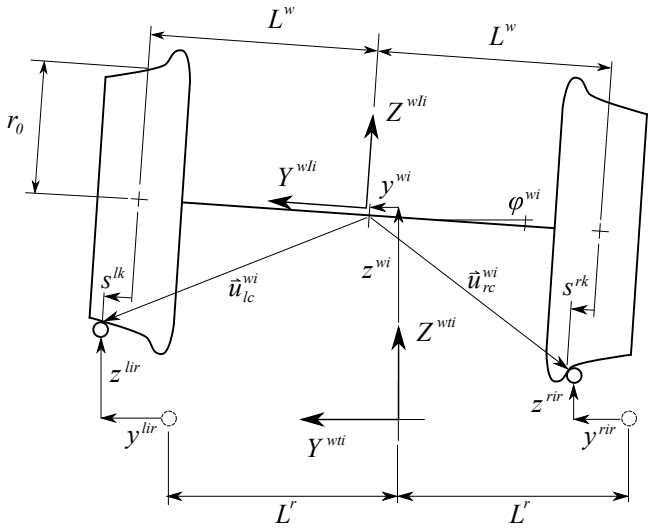

Figure 8: Wheelset with knife edge constraints

Using the same simplifying geometric assumptions described in Subsection 4.2, the generalized coordinates $\mathbf{q}^{wi}$ of a wheelset with KEC-constraints are subjected to the following non-linear equations:

$$\bar{\mathbf{r}}_{lc}^{wi}\left(\mathbf{q}^{wi}, s^{lk}\right) - \bar{\mathbf{r}}^{lir} = \mathbf{0} \tag{47}$$

$$\bar{\mathbf{r}}_{rc}^{wi}\left(\mathbf{q}^{wi}, s^{rk}\right) - \bar{\mathbf{r}}^{rir} = \mathbf{0} \tag{48}$$

Using again just the Y and Z components of these two equations, Eqs. 47-48 are a system of 4 non-linear algebraic equations that can be developed as follows:

$$\begin{aligned}
y^{wi} + s^{lk} + \varphi^{wi}\left[r_0 + f^{lk}\left(s^{lk}\right)\right] - y^{lir} = 0 \\
z^{wi} + \varphi^{wi}\left[L^w + s^{lk}\right] - f^{lk}\left(s^{lk}\right) - r_0 - z^{rir} = 0 \\
y^{wi} + s^{rk} + \varphi^{wi}\left[r_0 + f^{rk}(s^{rk})\right] - y^{rir} = 0 \\
z^{wi} + \varphi^{wi}\left[-L^w + s^{rk}\right] - f^{rk}\left(s^{rk}\right) - r_0 - z^{rir} = 0
\end{aligned} \tag{49}$$

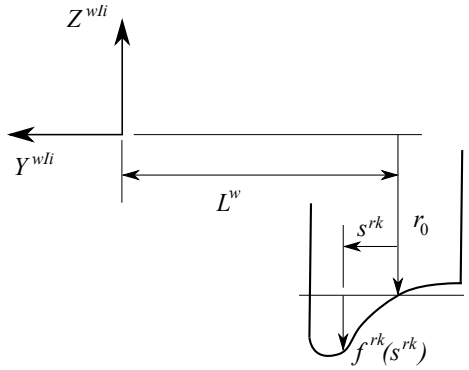

Figure 9: Right wheel equivalent KEC profile

where s^{lk} and s^{rk}, are the surface parameters associated with the left and right contact points in the wheel KEC profiles, respectively, and $f^{lk}(s^{lk})$ and $f^{rk}(s^{rk})$ are the functions that define the wheel KEC profiles at these points. Figure 9 shows a right wheel KEC profile. Equation 49 is a system of 4 equations that includes 2 new coordinates, s^{lk} and s^{rk}. Therefore, it eliminates $4 - 2 = 2$ degrees of freedom of the wheelset motion, as the general contact constraints

Eqs. 27-29 and the approximate contact constraints Eqs. 35-36 do. However, its structure is far simpler.

Defining the new wheelset vertical coordinate $\bar{z}^{wi} = z^{wi} - r_0$ is convenient because $\bar{z}^{wi}$ is a small-valued coordinate that is zero when the wheelset is centred ($y^{wi} = 0$). Using this new coordinate, the KEC constraints can be written in the following compact matrix form:

$$\begin{bmatrix} 0 & r_0 + f^{lk} & 1 & 0 \\ 1 & L^w & \varphi^{wi} & 0 \\ 0 & r_0 + f^{rk} & 0 & 1 \\ 1 & -L^w & 0 & \varphi^{wi} \end{bmatrix} \begin{bmatrix} \bar{z}^{wi} \\ \varphi^{wi} \\ s^{lk} \\ s^{rk} \end{bmatrix} + \begin{bmatrix} y^{wi} - y^{lir} \\ -f^{lk} - z^{lir} \\ y^{wi} - y^{rir} \\ -f^{rk} - z^{rir} \end{bmatrix} = \mathbf{0} \;\Rightarrow \tag{50}$$

$$\Rightarrow \; \mathbf{C}^{kec}\left(y^{wi}, \mathbf{x}^{wi}, \mathbf{x}^{ir}\right) = \mathbf{0}.$$

where $\mathbf{x}^{wi} = [\bar{z}^{wi} \quad \varphi^{wi} \quad s^{lk} \quad s^{rk}]^T$ are the wheelset dependent coordinates, f^{lk} and f^{rk} mean here the value of the KEC profiles at a particular value of the surface parameters s^{lk} and s^{rk}, this is, $f^{lk} = f^{lk}(s^{lk})$, $f^{rk} = f^{rk}(s^{rk})$, and the column array $\mathbf{x}^{ir} = [y^{lir} \quad z^{lir} \quad y^{rir} \quad z^{rir}]^T$ includes the left and right rail irregularities.

The use of the KEC-constraints equations of Eq. 50 in the dynamic simulation of railway vehicles is done under the assumption that for each wheelset the lateral coordinate y^{wi} is treated as independent while the vertical coordinate z^{wi} and the roll angle φ^{wi} are treated as dependent coordinates. Each time step the solver finds the values of y^{wi} and s^{wi} that are used to calculate the array of irregularities $\mathbf{x}^{ir}$. With that information, Eq.50 is solved to find the value of $\mathbf{x}^{wi}$ that includes the dependent coordinates. The following pseudo-code shows this procedure:

A. Coordinate partition for wheelset i:

$$\mathbf{q}^{wi} = \begin{bmatrix} \mathbf{q}^{wi}_{ind} \\ \mathbf{q}^{wi}_{dep} \end{bmatrix},$$
$$\mathbf{q}^{wi}_{ind} = \begin{bmatrix} s^{wi} & y^{wi} & \theta^{wi} & \psi^{wi} \end{bmatrix}^T$$
$$\mathbf{q}^{wi}_{dep} = \begin{bmatrix} z^{wi} & \varphi^{wi} \end{bmatrix}^T$$

B. Given the value of $\mathbf{q}^{wi}_{ind}$:

1. Find track irregularities: $\mathbf{x}^{ir} = \mathbf{x}^{ir}\left(s^{wi}\right)$
2. Solve Eq. 50 to find $\mathbf{x}^{wi}$
3. Extract $\mathbf{q}^{wi}_{dep}$ from $\mathbf{x}^{wi}$

This solution procedure (y^{wi} and $\mathbf{x}^{ir}$ are inputs and $\mathbf{x}^{wi}$ is output of Eq. 50) is highlighted here because there is an alternative solution procedure that is used to find the knife-edge equivalent profiles and explained in next section.

In the dynamic simulation the nonlinear Eq. 50 can be solved very efficiently using as initial guess:

$$\mathbf{x}^{wi}_0 = \begin{bmatrix} \dfrac{f^{lk}\left(-y^{wi}\right) + f^{rk}\left(-y^{wi}\right)}{2} & 0 & -y^{wi} & -y^{wi} \end{bmatrix}^T \tag{51}$$

that represents an approximate solution with zero roll angle.

The fourth row of Table 3 shows the level of simplification that is achieved when a wheelset is modelled with KEC constraints. As it can be observed, the simplification is comparable to the reduction to 2D contact from 3D contact explained in Section 4.2.

6. Knife-edge equivalent profiles

Real rail head profiles cannot be assumed as a single point. In real applications, the contact point location moves significantly across the rail head, particularly when the contact point moves from the tread to the flange of the

wheel. The position of the contact point in the wheel and rail profiles, for a set of values of the lateral displacement of the wheelset, can be observed at the left of Fig. 10. The wheel has S1002 profile and the rail head is LB-Area140 type. Clearly, there are two well separated contact zones in the tread and the flange of the wheel. In these two zones, the contact point moves significantly in the lateral direction of the rail head profile. Therefore, it is not realistic just to replace the original rail profile by a knife-edge profile, but also the original wheel profile has to be replaced by an equivalent profile in order to reproduce the constraint of the original profile combination. This wheel profile will be referred as the *knife-edge equivalent profile* in the following. A wheelset with knife-edge-equivalent profiles has a space of allowable motion that is the same that the real wheel in contact with the real *finite-width* rail head profile. Finding such a wheel profile would allow the use of the simple KEC-constraints given in Eq. 49 instead of the more complicated given in Eqs. 27-29 or in Eqs. 35-36. This section explains a method that can be followed to find the knife-edge-equivalent profiles. Figure 10 on the right shows the KEC-equivalent profile of the S1002 - LB-Area140 profiles combination. In the KEC-equivalent profile, the contact point moves continuously, without showing finite jumps in position, when the wheelset moves laterally in the track. Note that the two plots in Fig. 10 have different space-scales, being the KEC-equivalent profile much narrower that the real profiles.

The algorithm used to find the knife-edge equivalent profiles is based on the solution of the Eq. 50. In contrast to the solution procedure of equations explained at the end of last section, the solution procedure uses y^{wi}, $\mathbf{x}^{ir} = \mathbf{0}$, z^{wi} and φ^{wi} as the inputs and $[s^{lk},\ f^{lk}]$ and $[s^{rk}\ f^{rk}]$ as the outputs (four equations, four unknowns). The process starts by creating the contact lookup tables with the real wheel and rail profiles and no track irregularity. The contact lookup tables include the functions $z^{wi} = z^{clu}(y^{wi})$, $\varphi^{wi} = \varphi^{clu}(y^{wi})$ given in Eq. 43. For each value of y^{wi}, these functions produce one value of z^{wi} and φ^{wi}, which can be used as inputs to the KEC contact constraints given in Eq. 50. The

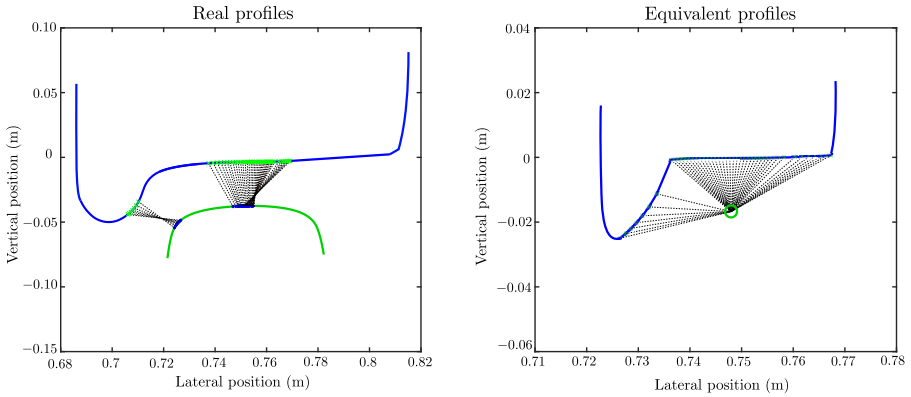

Figure 10: Contact points on wheel and rail profiles (left) and contact point on KEC-equivalent profile (right)

solution of these 4 equations provide 4 outputs: s^{lk}, s^{rk}, f^{lk} and f^{rk}. The following pseudo-code shows this procedure:

$y^{wi} = y^{wi}_{min} : \Delta y : y^{wi}_{max}$;
for i = 1:length(y^{wi})
    $z^{wi}(i)$ = zLookup($y^{wi}(i)$);
    $\varphi^{wi}(i)$ = phiLookup($y^{wi}(i)$);
    [s^{lk}(i), s^{rk}(i), f^{lk}(i), f^{rk}(i)] = solveKEC($y^{wi}(i)$, $z^{wi}(i)$,$\varphi^{wi}(i)$);
end

where 'zLookup' and 'phiLookup' are the lookup functions that evaluate Eq. 43 and 'solveKEC' is the function that solves Eq. 49 using the inputs and outputs explained above. The couples [s^{lk}(i), f^{lk}(i)] and [s^{rk}(i), f^{rk}(i)] can be used as lookup functions that provide the left and right KEC-equivalent profiles.

The method used to find the KEC equivalent profile guarantees the same value of the functions $z^{wi} = z^{clu}(y^{wi})$, $\varphi^{wi} = \varphi^{clu}(y^{wi})$ (space of allowable motion) for the selected values of the lateral displacement y^{wi} in a track without irregularities. However, the method does not guarantee that the space of al-

lowable motion is also coincident in the presence of irregularities. Obviously, the KEC equivalent profiles cannot be a function of the gauge variation gv as the contact lookup table does ($z^{wi} = z^{clu}(y^{wi}, gv)$, $\varphi^{wi} = \varphi^{clu}(y^{wi}, gv)$). The numerical results given next show the kinematics of the wheelset with KEC equivalent profiles in an irregular track compared with the one obtained with contact lookup tables. As shown in the example, the profile equivalence works fine for an irregular track too.

The KEC-method can be summarized as the use of fictitious profiles $f^{lk}(s^{lk})$ and $f^{rk}(s^{rk})$ that guarantee that, for a given set of values of the lateral displacement y^{wi} and the track irregularities $\mathbf{x}^{ir}$, the solutions of the constraints $\mathbf{C}^{kec} = \mathbf{0}$ given in Eq. 49 or 50 coincide with the functions $z^{wi} = z^{clu}(y^{wi}, gv)$, $\varphi^{wi} = \varphi^{clu}(y^{wi}, gv)$.

7. Calculation of wheel-rail normal contact forces with KEC-method

Dynamic simulation of railway vehicles with the KEC-method uses the constraint equations of Eq. 49 to account for the wheel-rail contact. The solution of these equations provide the vertical displacement z^{wi} and the roll angle φ^{wi} as a function of the lateral displacement y^{wi} and the rail irregularities. The solution of Eq. 49 provide also the position of the contact points on the KEC-equivalent profiles through the values of the wheel geometric parameters s^{lk} and s^{rk}. Clearly, these are fictitious contact points. Contact forces have to be applied at their position in the real profiles. The equivalence of the KEC-profiles is kinematic not dynamic.

Once the position of the contact point in the KEC-equivalent profile is found, the location of the contact points in the real wheel and rail profiles is easily obtained. When calculating the KEC-equivalent profile, as described in Section 6, the values of the surface parameters in the real profiles (s^{lw}, s^{lr}, s^{rw}, s^{rr})

and the values of the surface parameters in the equivalent profiles (s^{lk}, s^{rk}) are stored for each value of the lateral displacement y^{wi} to create the following lookup functions:

$$s^{lw} = s^{lw}\left(s^{lk}\right), \quad s^{lr} = s^{lr}\left(s^{lk}\right), \quad s^{rw} = s^{rw}\left(s^{rk}\right), \quad s^{rr} = s^{rr}\left(s^{rk}\right) \tag{52}$$

Being the inputs the surface parameters of the contact points in the KEC-equivalent profiles and the outputs the surface parameters in the real wheel and rail profiles.

Because the wheel-rail contact is modelled with (equivalent) constraint equations, the normal contact forces are determined as reaction forces in the equations of motion. Each wheel-rail contact has an associated Lagrange multiplier, that is unknown each time step, whose physical meaning is the magnitude of the normal contact force. In contrast to the usual procedure used in multibody dynamics, the generalized normal contact force is not obtained by multiplication with the transpose of the Jacobian of the constraint equations. The reason is that this procedure would require to eliminate first the surface parameters out of the constrain equations of Eq. 49. This is not an easy task. Instead of this, the generalized normal contact forces for each wheelset is computed as follows:

$$\mathbf{Q}^{wi}_{fcn} = \begin{bmatrix} \bar{\mathbf{n}}^{lrp}_c & \bar{\mathbf{n}}^{rrp}_c \\ \hat{\mathbf{u}}^{lrp}_c \times \hat{\mathbf{n}}^{lrp}_c & \hat{\mathbf{u}}^{rrp}_c \times \hat{\mathbf{n}}^{rrp}_c \end{bmatrix} \begin{bmatrix} \lambda^l_c \\ \lambda^r_c \end{bmatrix} \tag{53}$$

where λ^l_c and λ^r_c are the Lagrange multipliers associated with the left and right normal contact forces. These unknown forces are multiplied by a 2×6 matrix that contains the normal directions and the directions associated with the resulting torques. The inputs of this matrix are the local position vectors and the normal vectors to the real surfaces at the contact points. These vectors are obtained once the surface parameters in the real profiles are calculated with the functions provided in Eq. 52.

The tangential (creep) contact forces are computed in this investigation using method [26] because of its good balance between accuracy and computational efficiency. Therefore, tangential contact forces are treated as applied forces. In addition to the location of the contact points in the real profiles, the calculation of the tangential contact forces requires also the value of the normal contact forces, the normalized relative tangential velocities at the contact points (creepages) and the value of the Kalker's linear coefficients that in turn depend on the surfaces curvatures. All these variables that depend on the wheel-rail surfaces properties are computed at the real wheel-rail profiles.

8. Simulation results

In this section a numerical case study of the MS-vehicle (*Metro de Sevilla*) using the KEC-method is analysed and compared to results provided by the constraint formulation using contact lookup tables [5] explained in Section 4.3. To this end, this section is organized as follows: first, the mechanical properties of the MS-vehicle together with the real wheel-rail profile combination and its equivalent one using the KEC-method are presented. Then, the results of the MS-vehicle running on a track with irregularities are shown and compared to those obtained using the fully constraint approach of contact lookup tables. Finally, a computational efficiency comparison is presented as a closure.

8.1. Multibody model of MS-vehicle

The modelled vehicle is a typical light train (*light rail transit*, LRT) built by the Spanish company CAF. Figure 11 shows a sketch of the multibody model. The vehicle model includes a set of five carbodies (*c1* - *c5*) connected with spherical joints (*a1* - *a4*) permitting relative pitch and yaw motions of the carbodies without resistance and a relative roll limited by a rotational spring. The vehicle model also includes three bogie frames (*b1* - *b3*), two of which belong to drive-bogies (*b1* and *b3*) and the other, *b2*, belongs to a trailed bogie. Finally, the model includes six wheelsets with independently rotating wheels (IRW-wheelsets, *w1* - *w6*). In total, the resulting vehicle model has 84 DoFs.

Regarding the IRW-wheelsets, unlike other vehicles with IRW (like the Spanish train *Talgo*), the two wheels with independent rolling motion in the MS-vehicle are connected with bearings to a non-rotating component that is called in the industry *bridge* instead of *axle* because of its geometry. The IRW-wheelset does not require the definition of the wheelset intermediate frame used in this paper because the body frame of this bridge plays an equivalent role in the formulation. The use of the KEC-method with IRW-wheelset has no additional difficulties.

The vehicle suspension system includes primary suspension elements connecting the IRW-wheelsets with the bogie frames, secondary suspension elements connecting the bogie frames to the carbodies and coupling elements connecting the carbodies at their roofs above the spherical joints. It is also equipped with traction rods, which connect the carbodies to the bogie frames, that are modelled as force elements.

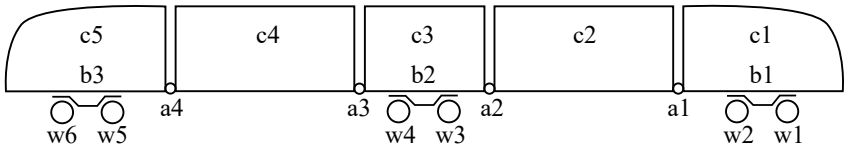

Figure 11: Schematic multibody model of MS-vehicle

Table 4 shows the mass properties of the vehicle. Simulations are done assuming a fully loaded vehicle. Table 5 shows the dimensions of the vehicle. The given lengths can be identified in Fig. 12. Note that the vehicle is geometrically symmetric but inertially non-symmetric.

8.2. MS-vehicle KEC equivalent wheel profile

The MS-vehicle uses the wheel-rail profile combination shown in Fig. 13; the UIC-54 rail profile and a wheel profile given by CAF company.

The transversal position of the contact point on the surfaces of wheel and rail, which are represented by the surface parameters s^w and s^r, respectively, as functions of the wheelset's lateral displacement y^{wi} are shown in Fig. 14.

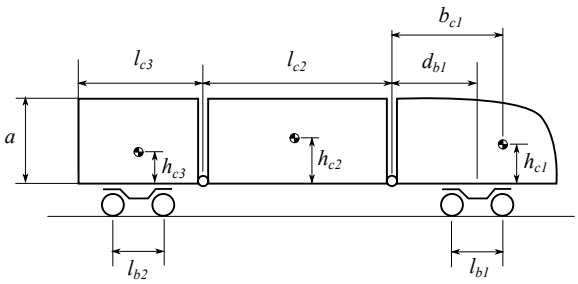

Figure 12: Main dimensions of MS-vehicle

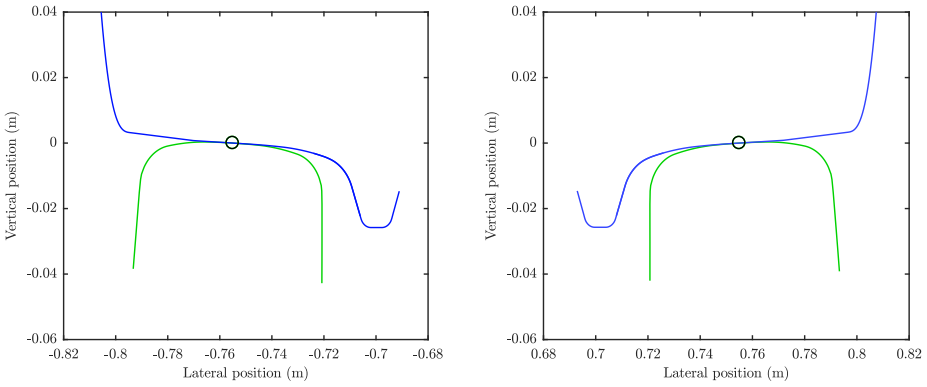

Figure 13: MS-vehicle real wheel-rail profile combination

Table 4: Vehicle masses (in kg)

Car body	**Empty mass**	**Passengers**	**Loaded mass**
1	6600	54	10380
2	6200	84	12080
3	3800	48	7160
4	5700	84	11580
5	6500	54	10280

Table 5: Vehicle dimensions (in mm)

l_{c3}	l_{c2}	d_{b1}	l_{b1}	l_{b2}	a	h_{c1}	h_{c2}	h_{c3}	b_{c1}
4404	6619	2203	1800	1800	3030	1291	1374	1346	2762

It should be pointed out that the original, non-worn profiles are used for the analysis. From the diagrams of Fig. 14, it can be seen that the functions are continuous so no abrupt contact jumps are observed.

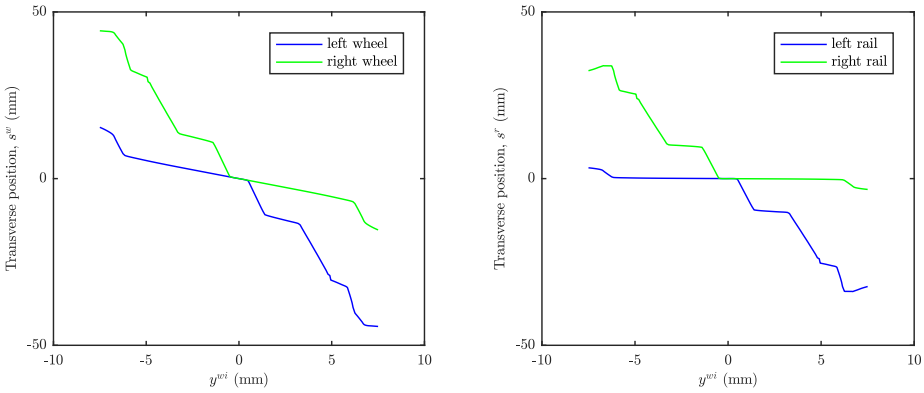

Figure 14: Contact point position on real profiles as a function of the wheelset lateral displacement. Left: position on wheel. Right: Position on rail. Blue line: Right wheel/rail. Green line: Left wheel/rail

The KEC equivalent wheel profile after applying the method proposed in Section 6, is shown in Fig. 15 and the wheelset kinematics given by both real and equivalent profiles is shown in Fig. 16. Results show that the KEC-equivalent

wheel gives the same wheelset kinematics that using real profiles.

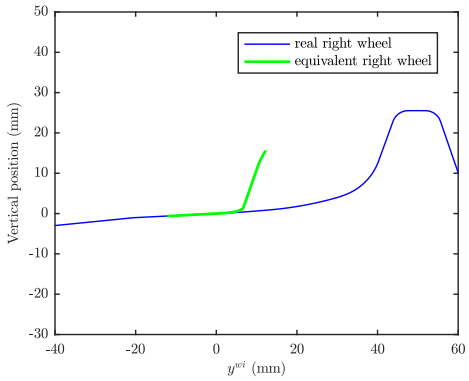

Figure 15: Comparison of real and equivalent right wheel profiles

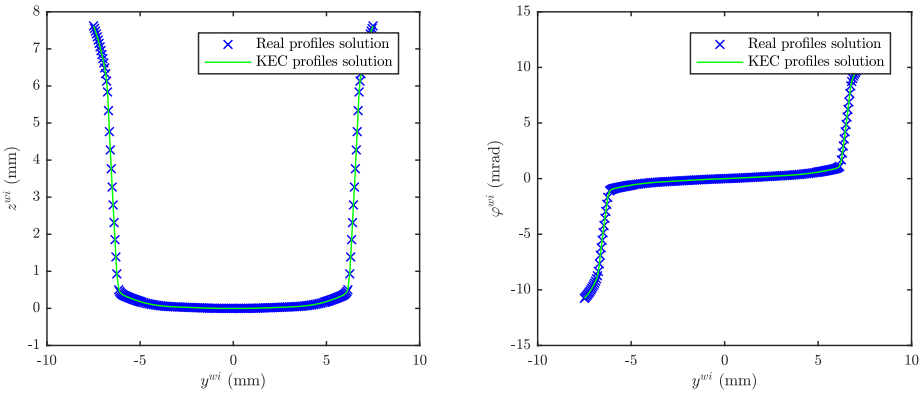

Figure 16: Wheelset kinematics using real and equivalent profiles

8.3. Case study: MS-vehicle on irregular track

With the purpose of validating the proposed method, the MS-vehicle running on an irregular track at a constant forward velocity of $V = 19$ m/s is simulated. The track has 1 km length and its horizontal profile is formed by a straight, transition and curve segments, as shown in Table 6, where $f_{lin}1$ and f_{lin}^2 are linear functions that vary between 0 and 1 along the length of the track segments. Vertical profile is completely horizontal.

Table 6: Track geometry parameters

Horizontal profile				
s_{range} [m]	Type	ρ_h [m^{-1}]	ρ_{tw} [rad]	ρ'_h [m^{-2}]
0-100	*Straight*	0	0	0
100-150	*Transition*	$f^1_{lin} \times 1/235.65$	$-1.5198 \cdot 10^{-3}$	$8.48716 \cdot 10^{-5}$
150-600	*Curve*	$1/235.65$	0	0
600-650	*Transition*	$f^2_{lin} \times 1/235.65$	$1.5198 \cdot 10^{-3}$	$-8.48716 \cdot 10^{-5}$
650-1000	*Straight*	0	0	0
Vertical Profile				
s_{range} [m]	Type		α_v [-]	ρ_v [m^{-1}]
1-1000	*Straight*		0	-

Figure 17 shows the four track irregularities of the track that have been generated using analytical expressions of the power spectral density functions (PSD) that can be found in literature. The procedure followed for this generation is described in [27].

Once the track ideal geometry and the irregularities are computed, the simulation of the MS-vehicle is carried out using both the KEC-method and the contact lookup tables method. The lateral displacement and the yaw angle of the vehicle bodies of the front bogie are presented in Fig. 18 together with their absolute difference when using both simulation methods. It can be observed that, when the vehicle enters the 235-m radius curve, wheelsets and bogie frames displace laterally to properly negotiate the curve. Due to the lateral irregularities, the wheelsets and frame do not reach a lateral stable position. It is also interesting to remark that, as expected in the dynamic behaviour of railway vehicles, the yaw angle of the front and rear wheelsets are opposite in sign when passing the curve due to the influence of the primary suspension. The resulting

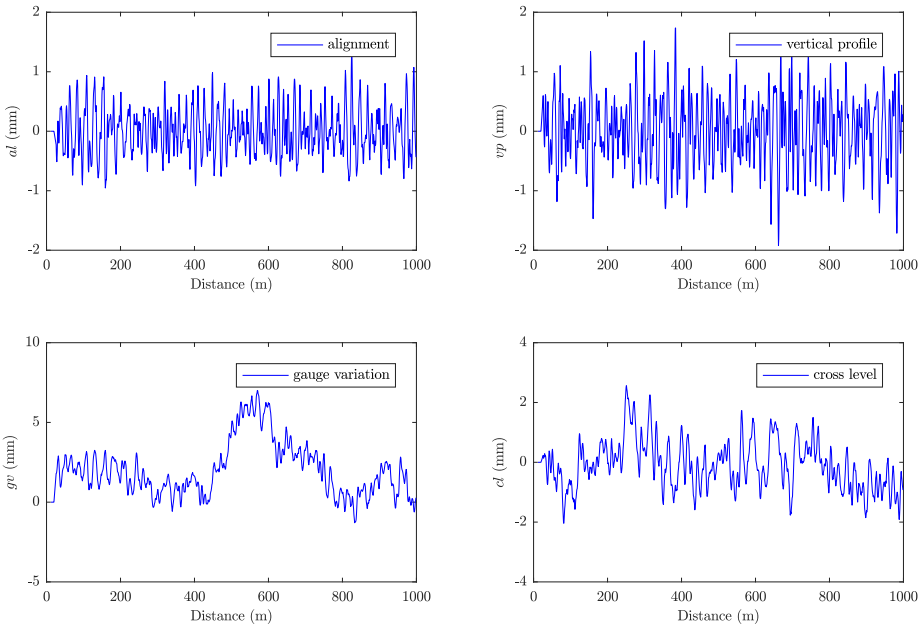

Figure 17: Track irregularities

lateral displacements and yaw angles are quite similar using both methods as it can be observed in the lower plots of Fig. 18. In the light of these results, the accuracy of the proposed method with respect to the use of lookup tables is clearly proven, since differences in lateral and yaw variables do not exceed the 1 mm and 0.5 mrad, respectively. As it can be observed in Fig. 18, the yaw angles of the wheelsets reach a maximum absolute value of 7 mrad. This value is smaller than the 16 mrad that was shown in Ref. [5] to have little effect in the position of the contact point with respect to the contact conditions with zero yaw angle. Therefore, neglecting of the influence of the yaw angle in the location of the contact points seems reasonable in the selected example.

As the vehicle negotiates the left curve, right wheels experience a higher normal contact forces than left ones as shown in the upper plots of Fig. 19. Here, the accuracy in contact forces is also achieved in terms of the absolute differences shown in the lower plots of Fig. 19.

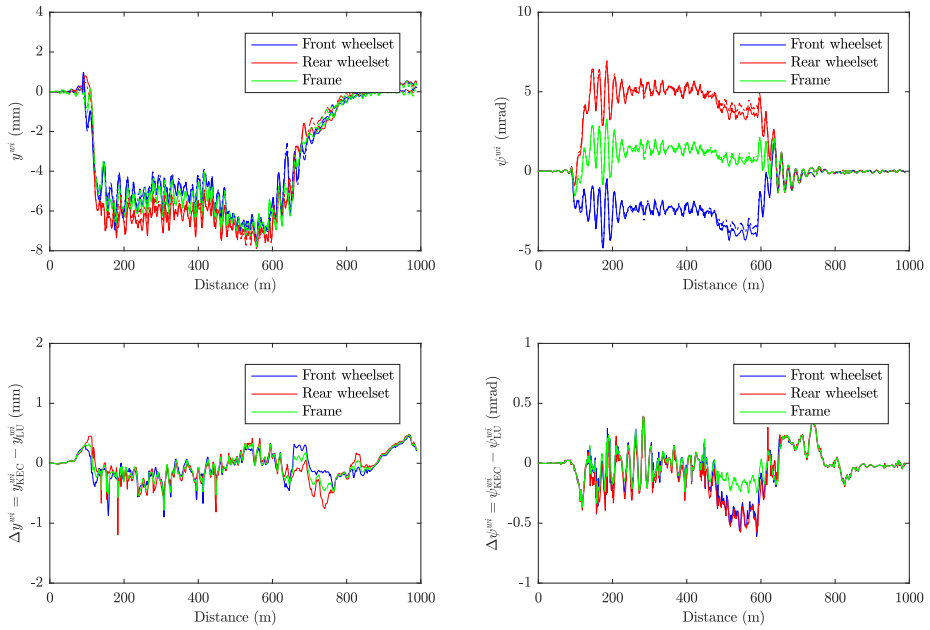

Figure 18: Kinematics results on front bogie. (y^{wi} = lateral displacement; ψ^{wi} = yaw angle). Solid line: Solution with KEC-method. Dashed line: Solution with contact lookup tables

8.4. KEC-method efficiency

The greater computational efficiency of the constraint contact method compared to the elastic contact method is well-known, as explained and referenced in the introduction of this paper. This is due to the absence of a contact points search algorithm and the avoidance of high frequency vibrations due to the Hertzian stiffness when using the former method. Because of that, being the KEC-method a constraint-based method, its computational efficiency is only compared in this work with other constraint-based method. In a previous paper of the authors [5], the on-line solution of the contact constraints was compared with the solution based on contact lookup tables. It was demonstrated that the later method was 6 times computationally faster than the former one when producing very similar results. Due to that reason, in this paper, computing times with the KEC-method are compared only with the use of constraint-based contact lookup tables.

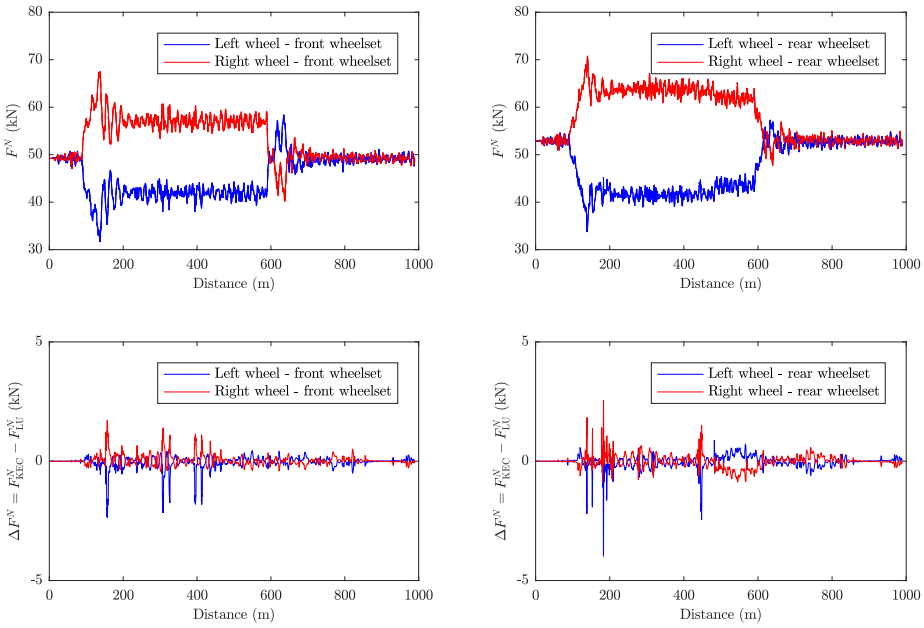

Figure 19: Case 2: Normal contact force (F^N) on wheels at front bogie. Solid line: Solution with KEC-method. Dashed line: Solution with contact lookup tables

Both models are implemented in Matlab R2016b running on a computer with processor Intel Core i7-6700HQ @ 2.60GHz. The adopted integrator is the adapted time-step size *ode15s* from Matlab and a maximum step size of 0.02 s is fixed. Table 7 shows the computational cost for the simulation of the two cases using both methods.

Table 7: Computational cost

	KEC-method	Lookup tables method
Computational time	347 s	434 s
Computational time / Real time	6.59	8.25

As shown in Table 7, the KEC-method reduces the computational cost up to 20% with respect to the efficient formulation of contact lookup tables. The table also shows the computational to real-time ratio. These rates can be greatly

improved if the computational codes were implemented using a low-level programming such as C/C++.

Recall that the simulation derived in this work refer to a 1 km track length with tangent, transition and curve segments where a full 84-DOF railway vehicle runs at a forward velocity of 19 m/s. In this context, Table 7 gives better computational times than the original work of contact lookup tables [5]. This is mainly due to the kinematic linearisation of railway vehicles presented in this work.

9. A note on the simulation of double contact points

In railway dynamic simulation it is commonly found combinations of wheel and rail profiles that result in finite jumps in the location of the contact points for certain values of the wheelset lateral displacement. When the wheelset adopts that particular value of the lateral displacement, there are two wheel-rail contact points (for example, tread contact and flange contact) instead of one. Simulation codes have to deal with this situation that is very important for curve negotiation analysis or derailment analysis.

It is difficult to use the constraint method for both the tread contact and the flange contact because the constraint functions are discontinuous at these points. Simulation of the double contact point scenario is easily done when using an elastic contact method. However, the elastic contact is not as efficient as the constraint method due to the high stiffness associated with the wheel-rail indentation. An alternative is the use of the hybrid method (constraint contact in the tread and elastic contact in the flange) [4]. However, the hybrid method is not an ideal solution because the numerical solvers have difficulties to deal with the impacts that appear due to the sudden appearance of contact points in the flange of the wheel. The quasi-elastic method mentioned in the introduction ([18], [19], [20]) is an alternative method to treat this situation efficiently.

The KEC-method presented in this paper has the potential to deal efficiently with double contact points using a contact constraint approach. It can be observed that, due to the knife-edge geometry of the rail in the KEC-method, the KEC-equivalent profiles do not show jumps in the location of the contact point when the real wheel-rail profiles do. This fact alleviates the continuity problems of the constraints in double contact point scenarios. However, the values of the normal contact forces (reactions) at each of the two contact points in this situation are not determined. This problem can be solved by further smoothing the KEC-equivalent constraints in the vicinity of the double contact point scenarios.

The treatment of double contact points with the KEC-method in no longer treated in this paper for the sake of brevity. It will be the subject of subsequent investigations. However, the efficient simulation of double contact points is one of the most important potential benefits of the used of the KEC-method.

10. Conclusions

This paper presents a new numerical procedure called *knife-edge-equivalent contact constraint method* (KEC-method) for the modelling and simulation of the wheel-rail contact in railway dynamic simulations. From the kinematic point of view, the method is based on the constraint approach and considers an equivalent wheel profile which contacts an ideal rail that has no lateral dimensions. For a realistic dynamic simulation, the KEC-method also allows to determine the exact position of the contact points in the real wheel-rail profile combination where the contact forces are applied. Compared to the use of contact lookup tables, the KEC-method allows the online calculation of the wheel-rail contact geometry with an improve in computational efficiency. In addition, it is shown that the KEC-method has the potential to deal with the double contact point scenario using continuous constraints equations. This will be the subject of a subsequent publication.

The proposed KEC-method for the wheel-rail contact is applied to simulate the *Metro de Sevilla* vehicle (metropolitan train of the city of Sevilla). The scenario in which the vehicle negotiates a 1 km length track is formed by tangent, transition and curve stretches with the inclusion of track irregularities. Numerical results are compared to those obtained using the efficient offline method of contact lookup tables. This comparison shows that the KEC-method is a reliable and efficient method that provides online and smoothed solution of the wheel-rail contact which reduces the computational cost up to 20% with respect to the use of contact lookup tables.

Acknowledgements

The first and third authors thank the Spanish Ministry of Science, Innovation and Universities under project reference TRA2017-86355-C2-1-R. Second author thanks the support given by the Spanish Ministry of Science, Innovation and Universities under the Mobility Program 'José Castillejo' with reference CAS18/00072. These supports are gratefully acknowledged.

Compliance with ethical standards

Conflicts of interest The authors declare that there is no conflict of interest to this work.

References

[1] A. A. Shabana, K. E. Zaazaa, H. Sugiyama, Railroad vehicle dynamics: a computational approach, CRC press, 2007.

[2] A. A. Shabana, M. Tobaa, H. Sugiyama, K. E. Zaazaa, On the computer formulations of the wheel/rail contact problem, Nonlinear Dynamics 40 (2) (2005) 169–193. doi:10.1007/s11071-005-5200-y.

[3] A. A. Shabana, J. R. Sany, An augmented formulation for mechanical systems with non-generalized coordinates: application to rigid body contact

problems, Nonlinear dynamics 24 (2) (2001) 183–204. doi:10.1023/A:1008362309558.

[4] A. A. Shabana, K. E. Zaazaa, J. L. Escalona, J. R. Sany, Development of elastic force model for wheel/rail contact problems, Journal of sound and vibration 269 (1-2) (2004) 295–325. doi:10.1016/S0022-460X(03)00074-9.

[5] J. L. Escalona, J. F. Aceituno, Multibody simulation of railway vehicles with contact lookup tables, International Journal of Mechanical Sciencesdoi:10.1016/j.ijmecsci.2018.01.020.

[6] J. C. Pombo, J. A. Ambrósio, Application of a wheel–rail contact model to railway dynamics in small radius curved tracks, Multibody System Dynamics 19 (1-2) (2008) 91–114. doi:10.1007/s11044-007-9094-y.

[7] M. Malvezzi, E. Meli, S. Falomi, A. Rindi, Determination of wheel–rail contact points with semianalytic methods, Multibody System Dynamics 20 (4) (2008) 327–358. doi:10.1007/s11044-008-9123-5.

[8] A. M. Recuero, J. F. Aceituno, J. L. Escalona, A. A. Shabana, A nonlinear approach for modeling rail flexibility using the absolute nodal coordinate formulation, Nonlinear Dynamics 83 (1-2) (2016) 463–481. doi:10.1007/s11071-015-2341-5.

[9] L. Baeza, D. J. Thompson, G. Squicciarini, F. D. Denia, Method for obtaining the wheel–rail contact location and its application to the normal problem calculation through 'contact', Vehicle System Dynamics (2018) 1–13doi:10.1080/00423114.2018.1439178.

[10] H. Sugiyama, K. Araki, Y. Suda, On-line and off-line wheel/rail contact algorithm in the analysis of multibody railroad vehicle systems, Journal of mechanical science and technology 23 (4) (2009) 991–996. doi:10.1007/s12206-009-0327-2.

[11] J. Santamaría, E. Vadillo, J. Gómez, A comprehensive method for the elastic calculation of the two-point wheel–rail contact, Vehicle System Dynamics 44 (sup1) (2006) 240–250. doi:10.1080/00423110600870337.

[12] G. Schupp, Bifurcation analysis of railway vehicles, Multibody System Dynamics 15 (2006) 25–50. doi:10.1007/s11044-006-2360-6.

[13] A. A. Shabana, M. Tobaa, B. Marquis, M. El-Sibaie, Effect of the linearization of the kinematic equations in railroad vehicle system dynamics, Journal of Computational and Nonlinear Dynamics 1 (1) (2005) 25–34. doi:10.1115/1.1951783.

[14] W. Zhai, X. Sun, A detailed model for investigating vertical interaction between railway vehicle and track, vehicle system dynamics 23 (S1) (1994) 603–615. doi:10.1080/00423119308969544.

[15] P. Fisette, J.-C. Samin, Lateral dynamics of a light railway vehicle with independent wheels, Vehicle System Dynamics 20 (sup1) (1992) 157–171. doi:10.1080/00423119208969395.

[16] P. Montenegro, S. Neves, R. Calçada, M. Tanabe, M. Sogabe, Wheel–rail contact formulation for analyzing the lateral train–structure dynamic interaction, Computers & Structures 152 (2015) 200–214. doi:10.1016/j.compstruc.2015.01.004.

[17] S. Muñoz, J. F. Aceituno, P. Urda, J. L. Escalona, Multibody model of railway vehicles with weakly coupled vertical and lateral dynamics, Mechanical Systems and Signal Processing 115 (2019) 570–592. doi:10.1016/j.ymssp.2018.06.019.

[18] M. Arnold, H. Netter, Wear profiles and the dynamical simulation of wheel-rail systems, in: Progress in Industrial Mathematics at ECMI 96, Springer, 1997, pp. 77–84. doi:10.1007/978-3-322-96688-9_8.

[19] G. Schupp, C. Weidemann, L. Mauer, Modelling the contact between wheel and rail within multibody system simulation, Vehicle System Dynamics 41 (5) (2004) 349–364. doi:10.1080/00423110412331300326.

[20] H. Netter, G. Schupp, W. Rulka, K. Schroeder, New aspects of contact modelling and validation within multibody system simulation of railway vehicles, Vehicle System Dynamics 29 (S1) (1998) 246–269. doi:10.1080/00423119808969563.

[21] J. F. Aceituno, R. Chamorro, D. García-Vallejo, J. L. Escalona, On the design of a scaled railroad vehicle for the validation of computational models, Mechanism and Machine Theory 115 (2017) 60–76. doi:10.1016/j.mechmachtheory.2017.04.015.

[22] F. Marino, A. Distante, P. L. Mazzeo, E. Stella, A real-time visual inspection system for railway maintenance: automatic hexagonal-headed bolts detection, IEEE Transactions on Systems, Man, and Cybernetics, Part C (Applications and Reviews) 37 (3) (2007) 418–428. doi:10.1109/TSMCC.2007.893278.

[23] G. Perrin, C. Soize, D. Duhamel, C. Funfschilling, Track irregularities stochastic modeling, Probabilistic Engineering Mechanics 34 (2013) 123–130. doi:10.1016/j.probengmech.2013.08.006.

[24] A. Wickens, Fundamentals of rail vehicle dynamics. Guidance and stability, CRC Press, 2005.

[25] C. Esveld, Modern Railway Track, MRT-Productions, 2001.

[26] O. Polach, Creep forces in simulations of traction vehicles running on adhesion limits, Wear 258 (2005) 992–1000. doi:10.1016/j.wear.2004.03.046.

[27] H. Claus, W. Schiehlen, Modeling and simulation of railway bogie structural vibrations, Vehicle System Dynamics 29 (S1) (1998) 538–552. doi:10.1080/00423119808969585.